On the relevance of turbulent structures resolution for cross-flow in a helical-coil tube bundle

Jinyong Feng[1], Michael Acton[1], Emilio Baglietto[1,*], Adam R. Kraus[2], Elia Merzari[2]

[1]*Massachusetts Institute of Technology, Cambridge, 02139, Massachusetts, USA*

[2]*Argonne National Laboratory, Lemont, 60439, Illinois, USA*

Abstract:

Helical-coil steam generators are being adopted in a number of advanced nuclear reactor designs because of their increased heat transfer efficiency and compactness. Due to the limited operational experience and the expected high cost of dedicated experiments, it is imperative to demonstrate the modeling capability. Computational fluid dynamics is ideally suited for this problem, due to its high resolution and accuracy. However, traditional low-cost URANS turbulence models have shown limited applicability for cross-flow in helical tube bundles. On the other hand, LES methods provide high-accuracy and high-fidelity data with prohibitively high computational cost for design use. In this work, the recently proposed hybrid second-generation model STRUCT is compared to classic URANS turbulence formulations against high-fidelity LES simulations. The STRUCT model produces accurate predictions for all relevant quantities, demonstrating high potential for reproducing helical-coil tube bundle flow phenomena accurately, at an affordable computational cost.

Keywords: helical tube, steam generator, STRUCT, URANS, LES, wall function

1. Introduction

The design of steam generators has significant impact on nuclear reactor operation and safety. Classic straight tube steam generators have been the standard in the nuclear industry. However,

* Corresponding author. Tel,: +1 617 253 4231
E-mail address: emiliob@mit.edu (Emilio Baglietto)

helical tube bundle designs are generating renewed interest due to their compactness and efficient heat transfer. Early studies have shown that for the same flow rate and inlet fluid temperatures, the heat transfer coefficient can be increased by up to 43% (Prabhanjan et al., 2002) while also reducing vulnerability to thermal expansion and stress issues common in straight tube designs (Carelli et al., 2004). Such advantages make helical steam generators an ideal candidate for small modular reactor concepts, where reliability and size are at a premium. In order to ensure reliability and performance, a robust understanding of the structural dynamics and associated flow phenomena is necessary.

Since the primary coolant flows around the steam generator tubes, the pressure drop characteristic and the heat transfer efficiency are closely related to the geometric configuration and size of the tube bundles. While general design criteria are available, detailed experimental data and operating experience for helical steam generators are far more limited than for other more common geometries, such as straight-tube or U-tube designs. Thus at the current time, large uncertainties must be taken into account in helical tube steam generator design, and these uncertainties propagate to other aspects of the plant design process. Constructing new experiments, particularly at prototypical scales and operating conditions, can be very costly.

Another aspect crucial to the industrial adoption of helical steam generator is their mechanical performance throughout the long operating life of the plant. Among the drivers of tube failures flow-induced vibration (FIV) is one of the most notable and challenging to prevent. The structural response of the tubes is closely related to the load induced by the flow condition. To estimate FIV, it is imperative to extract the load on the structure from the mean and fluctuating components of the flow fields, which has been difficult to measure in physical experiments.

Numerical modeling, primarily through computational fluid dynamics (CFD) approaches, is a natural complement to existing experimental data. Validated and verified CFD models can be used to reduce the amount of testing needed to characterize a system, providing substantial reduction in the overall design cost, and in some cases providing data that would be difficult to obtain experimentally. As a first principle-based approach, direct numerical simulation (DNS) resolves the turbulent eddies down to the finest Kolmogorov scale, thus capturing all 3D flow features; Large Eddy Simulation (LES) can also provide high-fidelity data by resolving most of the energetic scales of turbulence. Therefore, in theory, both DNS and LES approaches could be leveraged to complement the experiment datasets and provide high-fidelity reference data.

However, both approaches are still computationally too expensive and impracticable for prototypical steam generator design. Compared to DNS and LES approaches, Reynolds-averaged Navier Stokes (RANS) turbulence models, which solve for the averaged flow behavior, can often provide acceptable results at presently affordable computational cost, making it attractive for design applications. However, RANS models have several well-known limitations that restrain their generality, and which can introduce significant uncertainties in the flow solution. RANS models in particular fail to capture the large coherent turbulent structures that can be present in conjunction with high local shear and flow separation, and which can have a dominant influence on the magnitude of the velocity and temperature fluctuations. In the present tube bundle configuration, the flow going across the helical-coiled tubes will separate generating large local flow structure that are not explicitly resolved by RANS models, but are the main contributor to the forces leading to FIV. A similar phenomenon is observed in T-junction configurations, where the unsteady flow structures have major impact on thermal fluctuation (Feng et al., 2018a and 2018b).

The present work first assesses the performance of the most widely adopted Unsteady RANS (URANS) turbulence modeling approaches on the simulation of cross flow around the helical tube bundle. A recently proposed STRUCTure-based (STRUCT) second-generation URANS turbulence model (Lenci, 2016) is then evaluated, and aims at overcoming the limitations of URANS approaches by enhancing the resolution of unsteady turbulent structures. The results for pressure drop and velocity fields are compared against the reference LES data. The ultimate goal is to demonstrate a consistent mesh strategy and best practices for turbulence model applicability, thus enabling efficient design of helical-coil steam generators.

2. Turbulence Models Formulation

The theoretical background of the turbulence models adopted in the present study is briefly described in this section. As the most widely adopted turbulence closure family in industrial applications, a number of Unsteady Reynolds-averaged Navier-Stokes (URANS) models are investigated in this paper.

The Reynolds-averaged Navier-Stokes (RANS) models rely on the assumptions that its modeling variables, such as the velocity $\boldsymbol{u}$, can be decomposed as the sum of a mean quantity and a fluctuating term.

$$\boldsymbol{u}(\boldsymbol{x},t) =< \boldsymbol{u}(\boldsymbol{x},t) > +\boldsymbol{u}'(\boldsymbol{x},t) \qquad (1)$$

where $\boldsymbol{u}(\boldsymbol{x},t)$ is the instantaneous velocity for position $\boldsymbol{x}$ at time t.

RANS models were originally developed for steady-state simulations, in which the turbulent fluctuations are statistically stationary, so that resolved flow variables are constant in time, while the statistical effect of residual scales is modeled. When moving from RANS to URANS, the statistics introduced for RANS are assumed to be valid in time-dependent flow cases. The underlying requirement of statistically stationary residual turbulence implies that variation of the resolved variables is slow compared to residual turbulent fluctuations. The term slow indicates that a spectral gap should exist between resolved and modeled frequencies. In complex flow, where strong flow deformation occurs, the assumption of time-scale separation for RANS/URANS no longer holds, and a substantial interaction between the unresolved turbulent fluctuations and the resolved fluctuations occurs. For the unsteady version of the RANS model, a finite-time temporal average is used and the instantaneous velocity $\boldsymbol{u}$ is

$$\boldsymbol{u}(\boldsymbol{x},t) =< \boldsymbol{u}(\boldsymbol{x},t) > +\boldsymbol{u}'(\boldsymbol{x},t) \qquad (2)$$

The difference between RANS and URANS is that an additional unsteady term is present in the URANS momentum equations. The mean quantities are no longer time-independent but defined as the superposition of a temporal average $< \overline{\boldsymbol{u}(\boldsymbol{x})} >$ and the resolved fluctuating component $\boldsymbol{u}''(\boldsymbol{x},t)$ of the mean velocity. Thus

$$\boldsymbol{u}(\boldsymbol{x},t) =< \overline{\boldsymbol{u}(\boldsymbol{x})} > +\boldsymbol{u}''(\boldsymbol{x},t) + \boldsymbol{u}'(\boldsymbol{x},t) \qquad (3)$$

where $\boldsymbol{u}(\boldsymbol{x},t)$ is the instantaneous velocity for position $\boldsymbol{x}$ at time t, $< \overline{\boldsymbol{u}(\boldsymbol{x})} >$ and $\boldsymbol{u}''(\boldsymbol{x},t)$ are the temporally averaged and resolved fluctuating part of the mean velocity, respectively, and $\boldsymbol{u}'(\boldsymbol{x},t)$ is the modeled fluctuating velocity. Then the total turbulent kinetic energy is defined as

$$k_{tot} = \frac{1}{2}(u_i'u_i' + u_i''u_i'') \qquad (4)$$

In the URANS models, the unknown terms are named Reynolds stresses and require closure:

$$\tau_{ij} = \rho\overline{u_i'u_j{}'} \qquad (5)$$

Following the original proposal from Boussinesq (Boussinesq, 1877), the Reynolds stress tensor, τ_{ij}, can be modeled with a simple linear proportionality to the mean strain rate tensor, $\overline{S_{ij}}$

$$\tau_{ij} = \frac{2}{3}k\delta_{ij} - 2\nu_t\overline{S_{ij}} \qquad (6)$$

where k is the turbulent kinetic energy and equal to $\frac{1}{2}(u_i'u_i')$. ε is the turbulent dissipation rate and defined as $\nu\left(\frac{\partial u_i'}{\partial x_k}\frac{\partial u_i'}{\partial x_k}\right)$. δ_{ij} is the Kronecker delta and defined as

$$\delta_{ij} = \begin{cases} 0, if\ i \neq j \\ 1, if\ i = j \end{cases} \tag{7}$$

The turbulent eddy viscosity, ν_t, is defined for dimensional reasons as:

$$\nu_t = C_\mu \frac{k^2}{\varepsilon} \tag{8}$$

The original standard $k-\varepsilon$ model (Jones and Launder, 1972; Launder and Sharma, 1974) relies on a linear relation between residual anisotropic stresses and strains in the resolved flow field. This simple relation is notably insufficient to describe complex strain, and fails in flows where curvature, rotation, stagnation or secondary flows are present.

Pope (Pope, 1975) proposed a more general non-linear eddy-viscosity model (NLEVM) formulation as an explicit algebraic simplification of the complete stress strain correlation. Residual anisotropic stresses in this approach are described by a polynomial formulation which is function of the turbulent kinetic energy (k), turbulent dissipation rate (ε), and other invariants derived from the resolved velocity gradient tensor. Among the numerous NLEVM closures that have been proposed in the literature, here we select the cubic formulation of Baglietto and Ninokata (Baglietto and Ninokata, 2006), which is based on the original proposal of Shih, Zhu and Lumley (Shih et al., 1995) as later extended by Lien et al. (Lien et al., 1996). The selected model was assembled to achieve general robustness and improve description of anisotropy in several test cases, including flow in nuclear fuel bundles (Baglietto et al., 2006; Baglietto and Ninokata, 2005).

The realizable $k-\varepsilon$ model (Shih et al., 1994) is also tested because it is the one of the most widely used URANS turbulence model and has a wide range of validation basis. It contains a modified transport equation for the turbulent dissipation rate ε. The critical coefficient of the model, C_μ, is expressed as a function of mean flow and turbulence properties, rather than assumed to be constant as in the standard model. This procedure allows the model to satisfy fundamental mathematical constraints on the normal stresses consistently with the physics of turbulence (realizability). However, it still relies on the isotropic turbulence assumption which in general is a simplification in most turbulent flows.

The $k-\omega$ shear stress transport (SST) (Menter, 1994) and lag elliptic blending (lagEB) $k-\varepsilon$ model (Revell et al., 2006) are also investigated here. For these two models, the treatment of turbulence in the bulk flow is relatively similar to the standard $k - \varepsilon$ model, but differs in the near wall turbulence treatment. The SST model blends a standard $k - \varepsilon$ model in the bulk flow with a $k - \omega$ model near the wall. The SST model has been widely used in the aerospace industry, where viscous flows are typically resolved and turbulence models are applied throughout the boundary layer. The lag elliptic blending model combines the standard elliptic model (Durbin, 1993; Manceau and Hanjalić, 2002) with the stress-strain lag concept originally proposed by Revell et al. (Revell et al., 2006). It incorporates additional terms to model the effects of anisotropy and provides a good predictive capability for separated or unsteady flow (such as vortex shedding), or when the flow is subject to rotation or strong streamline curvature.

Recently, a STRUCTure-based (STRUCT) second-generation URANS turbulence model was proposed (Lenci, 2016), which relies on the baseline cubic $k - \varepsilon$ model, along with locally adaptive time scale based resolution of relevant turbulent structures. These turbulent structures are identified by evaluating the second invariant of the velocity gradient tensor in the resolved field, representing the resolved time scales of the turbulence, and comparing it to the averaged model time scales. In region where the timescales overlap, the turbulent viscosity is reduced in order to increase turbulence resolution. The model extends the Baglietto and Ninokata nonlinear eddy-viscosity URANS formulation using a differential Lagrangian operator that transports a locally computed average time scale needed to obtain full closure. In order to ensure robustness, the model addresses the potential instability deriving from filtering at large time scales by reverting to the stable baseline URANS in flow locations with low flow deformation, for which the baseline URANS model is most reliable. As such, the STRUCT model has been designed to achieve robust accuracy on URANS type meshes. This adaptive scale resolution is enabled by an additional transport equation, increasing the computational cost over URANS by approximately 10% (Lenci, 2016). Demonstrations of the STRUCT model capabilities have been presented for thermal mixing in T-junctions (Feng et al., 2018b) and triple-jet (Acton et al. NURETH) configurations, flow past a square cylinder (Lenci, 2016), and flow through an asymmetric diffuser (Lenci, 2016).

The reference LES calculation used in the current work was performed using Nek5000 (Fisher et al., 2008), a massively-parallel spectral-element code developed at Argonne National Laboratory. LES with Nek5000 has been successfully demonstrated on a number of nuclear-relevant problems (Merzari et al., 2017), and has shown excellent scaling behavior. A mesh of roughly 3,000,000 elements was generated, which combined with a polynomial order of 7 yields over 1.5 billion degrees of freedom for the calculation. With this mesh, more than 99% near wall points have y^+ less than 1. Given the size of the domain, the turbulence cascade behavior, and the FIV validation, the mesh and data were deemed acceptable (Yuan et al., 2017). This allows the LES calculation to be used with confidence as high-fidelity validation data for URANS methods.

3. Numerical setup

All the non-LES simulations discussed in this paper are performed with the general-purpose commercial finite volume solver, STAR-CCM+ version 12.02 ("STAR-CCM+, version 12.02," 2017). The detailed information about the numerical setup for the CFD simulations are provided in this section.

3.1. Solution algorithms

A segregated flow solver is used, based on the SIMPLE algorithm and is applied on co-located variables using Rhie-Chow interpolation. A second order three-time level implicit time integration technique is applied, and the convective terms are interpolated by a non-oscillatory second-order upwind scheme for URANS and STRUCT models. A hybrid Gauss-least square method is used for computing reconstruction gradients, with the Venkatakrishnan reconstruction gradient limiter. Fluids are simulated assuming constant density and molecular viscosity.

To reduce the time integration error, the timestep size, Δ_t, for URANS models is set as 0.001 s, which ensures an average Courant-Friedrichs-Lewy (CFL) number less than 1. Previous studies (Feng et al., 2018a and 2018b) demonstrate that STRUCT model can adopt the same timestep size as URANS model and the solutions are consistent with CFL number up to 5. For all presented results, the physical time of the simulations is 4 s and the sampling window covers the range from 1 to 4 s, which represents approximately 5.6 flow-throughs (the time required for one Lagrangian particle to pass through the entire helical tube bundle region). In the SIMPLE algorithm, 7 outer iterations are used per timestep, thus having 28,000 iterations for the entire simulation. Although the pressure drop reaches its developed value relatively quickly, the turbulent kinetic energy takes longer to develop. In order to obtain useful statistics in a reasonable timeframe, volume averages over each subdomain shown in Figure 1 are used to compare the TKE between methods. Figure

1(a) shows the cross-section of two sample volumes. These volumes are located at the azimuthal center of the flow channels, and span 4.5° (10%) of the sector. The volumes are denoted by channel number, as shown in Figure 1(b). Channel 1 is the innermost radially (not including the sector wall channel), and Channel 6 is the outermost. Channels 1 and 4 have staggered arrangements while Channels 2 and 6 have in-line arrangements. Channels 1, 2, 4, and 6 are used for comparison in this work, with 29 "subchannel" volumes in the axial direction for each flow channel.

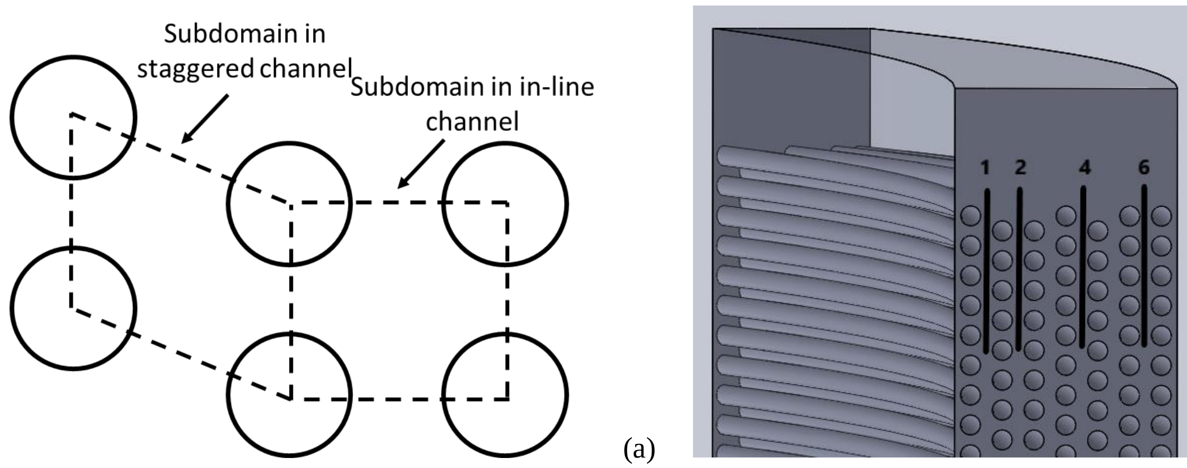

(a) (b)

Figure 1. Illustration of the data sampling volume. (a) shows the example subdomains used for TKE averaging in the in-line and staggered channel arrangements. (b) shows the flow channel numbering in the CFD domain [23].

The time-averaged mean velocity at a given volume is

$$\bar{V} = \frac{1}{N}\sum_{i=1}^{N} V_i \tag{9}$$

where N is the number of step and V_i is the instantaneous velocity at a given timestep, i.

The velocity variance is defined by the root mean square (RMS) as

$$\overline{V_{RMS}} = \sqrt{\frac{1}{N}\sum_{i=1}^{N}(V_i - \bar{V})^2} \tag{10}$$

3.2. Geometrical configurations

The helical geometry used in this work represents the physical configuration of the experiment performed at Argonne National Laboratory by Chen et al. (Chen et al., 1983). The geometry (Figure 2) is that of a half-scale, 135° azimuthal sector model of a liquid metal fast breeder reactor (LMFBR) design. There are 30 tube rows in the flow direction and 7 tube rows radially with a 1" (2.54 mm) pitch between columns. Four hanger bars support the tubes and separate the geometry into three azimuthal sectors of 45° each. The tubes extend slightly past the hanger bars and are open to the environment. Tests were performed in both air and quiescent water to establish the characteristic tube vibrational frequencies in these media. Flow tests were also performed, with flow only in the centermost sector. The flow originates at the inlet in the top and progresses to the outlet at the bottom. This center sector is the computational domain for the analyses in this work, as shown in Figure 3. The surfaces directly above and below the tubes are non-physical baffle surfaces for meshing purposes only.

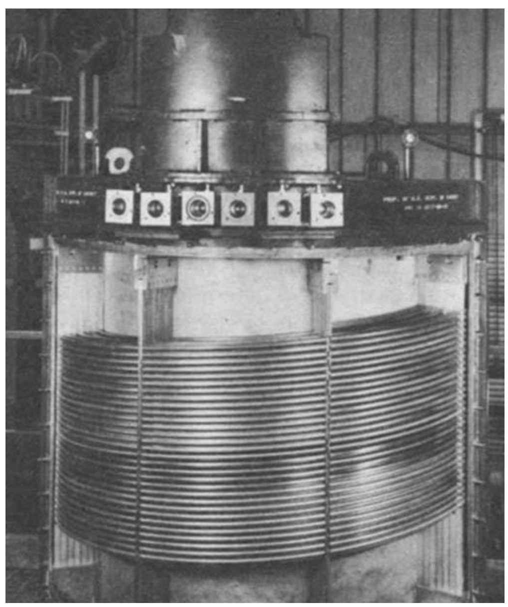

Figure 2. Helical tube bundle experiment investigated in current work (Chen et al., 1983).

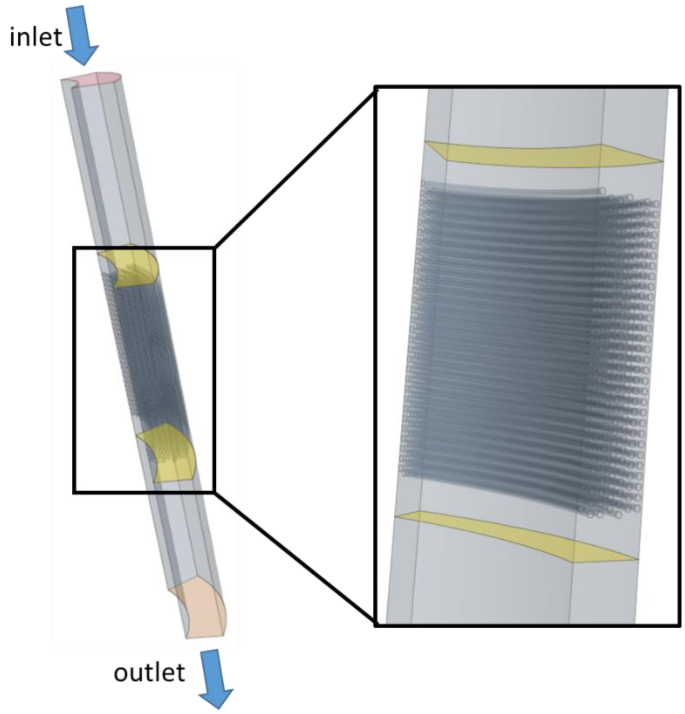

Figure 3. CFD simulation domain where the yellow planes represent the interfaces between each section

3.3. Initial and boundary conditions

In Chen's experiment (Chen et al., 1983), a screen flow equalizer was placed at the inlet of the test section, which produced a fairly uniform flow velocity distribution. In the simulation, a uniform inflow velocity of 0.49 m/s is adopted as the inflow boundary condition, which corresponds to 1.28 m/s "gap velocity" in the helical tube channels. This can be used to define a Reynolds number for the channels:

$$Re_{gap} = \frac{\rho V_{gap} D}{\mu} \qquad (11)$$

where ρ is the liquid density, V_{gap} is the gap velocity, D is the tube diameter with value of 0.0159 m, and μ is the liquid dynamic viscosity. The simulated 0.49 m/s velocity, corresponds to a Reynolds number of 20,352, and is lower than the reported velocity range (0.78~ 3.36 m/s) in Chen et al.' experiment (Chen et al., 1983) which has a corresponding prototypical Reynolds number from 32,397 to 13,9557. The reason for the reduced velocity is related the computational cost associated with the wall resolved LES simulations in NEK5000 for high Reynolds number. Since detailed measurements of the velocity fields around the helical tube are not available for the experimental conditions, LES represents the best validation available for the turbulence models selection, and the Reynolds number of 20,352 allows a large saving in simulation time while retaining the features of the flow configuration. The water is assumed to be isothermal at room temperature, so the liquid density of 998 $\frac{kg}{m^3}$ and dynamic viscosity of 0.001 $Pa \cdot s$ are used. No-slip boundary conditions are applied on the wall and the helical tube surfaces. Pressure outlet boundary condition are applied on the bottom outlet surface.

3.4. Mesh configurations

Accurate prediction of the near wall flow behavior is important to resolve the turbulent mixing phenomena. In this paper, we adopt the "two-layer" wall y^+ treatment approach for all tested URANS models. The "two-layer" wall treatment is a hybrid treatment that approximates the low-y^+ wall treatment for fine meshes (wall boundary y^+~ 1), and the high-y^+ wall treatment for coarse meshes (wall boundary y^+> 30). It is also formulated with the desirable characteristic of producing reasonable answers for intermediate mesh resolution. A blending function is used to calculate turbulence quantities such as dissipation and production of turbulent kinetic energy, and stress tensor for the buffer region of the boundary layer.

As shown in Figure 3, the simulation domain is separated into three regions, the top region above the helical tubes, the helical tube bundle region and the bottom region below the helical tubes. Since the flow behavior in the top and bottom regions is rather less complex and has marginal impact on the flow fluctuation in the steam generator regions, a coarse and uniform mesh resolution of 12 mm is applied there. For the helical tube bundle region, an unstructured 2D quadrilateral mesh was generated and swept along the helical angle to yield hexahedra. The first cell near the wall has wall y^+ from 1.7 to 31.82, thus the total number of cells ranges from 35.2 to 27.5 million, respectively. Statistics of the mesh configuration are provided in Table 1. The objective during mesh generation was to provide a reference for the assessment of the mesh sensitivity of the STRUCT model. By accurately capturing the flow separation on the wall, fine boundary layers (wall y^+~ 1) should be able to generate the best predictions compared to the reference solution, albeit at significantly increased computational cost. The idealized boundary layer resolution of ~10-20 cells would not be computationally practical for prototypical applications. Instead, in order to balance the increased cost with improved accuracy, the boundary layer growth rate is defined as 3.0 or 3.2, thus having respectively 3 or 4 boundary layers. The cross-sectional view of the mesh configuration near the helical tubes are given in **Figure 4** and the wall y^+ distribution for the three mesh configurations are given in **Figure 5**, where the STRUCT model was used to quantify the wall y^+. Adopting a different turbulence model has a negligible effect on the wall y^+ value, and STRUCT, standard $k - \varepsilon$ linear and standard $k - \varepsilon$ cubic produce values within a 2% variation range.

Table 1.

Statistics of the mesh configuration.

Meshing parameters	#1	#2	#3
Number of cells (millions)	27.5	31.4	35.2
Bulk mesh resolution (mm)	12	12	12
Thickness of the entire boundary layers (mm)	2.5	2.5	2.5
Number of boundary layers	2	3	4
Growth rate of boundary layers thickness	1.05	3.00	3.20
Averaged wall y^+ on the helical tube surfaces	31.82	6.34	1.69

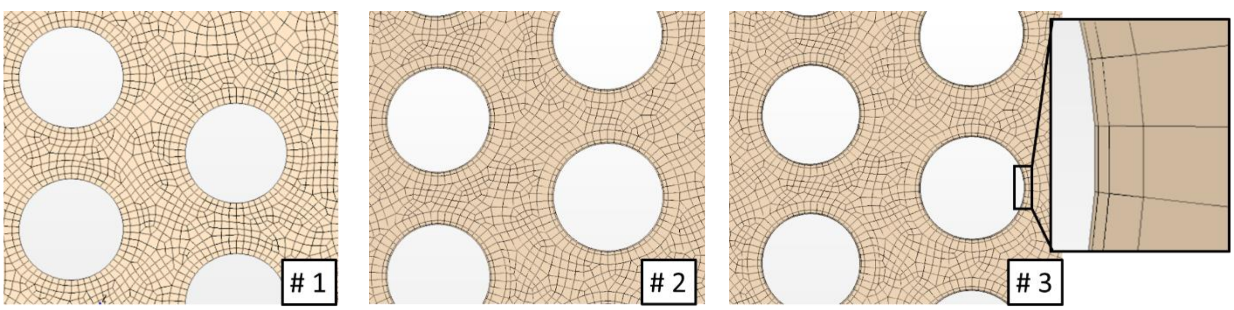

Figure 4. Cross-sectional view of the mesh configuration near the helical tubes for three different wall boundary layer setups given in Table 1.

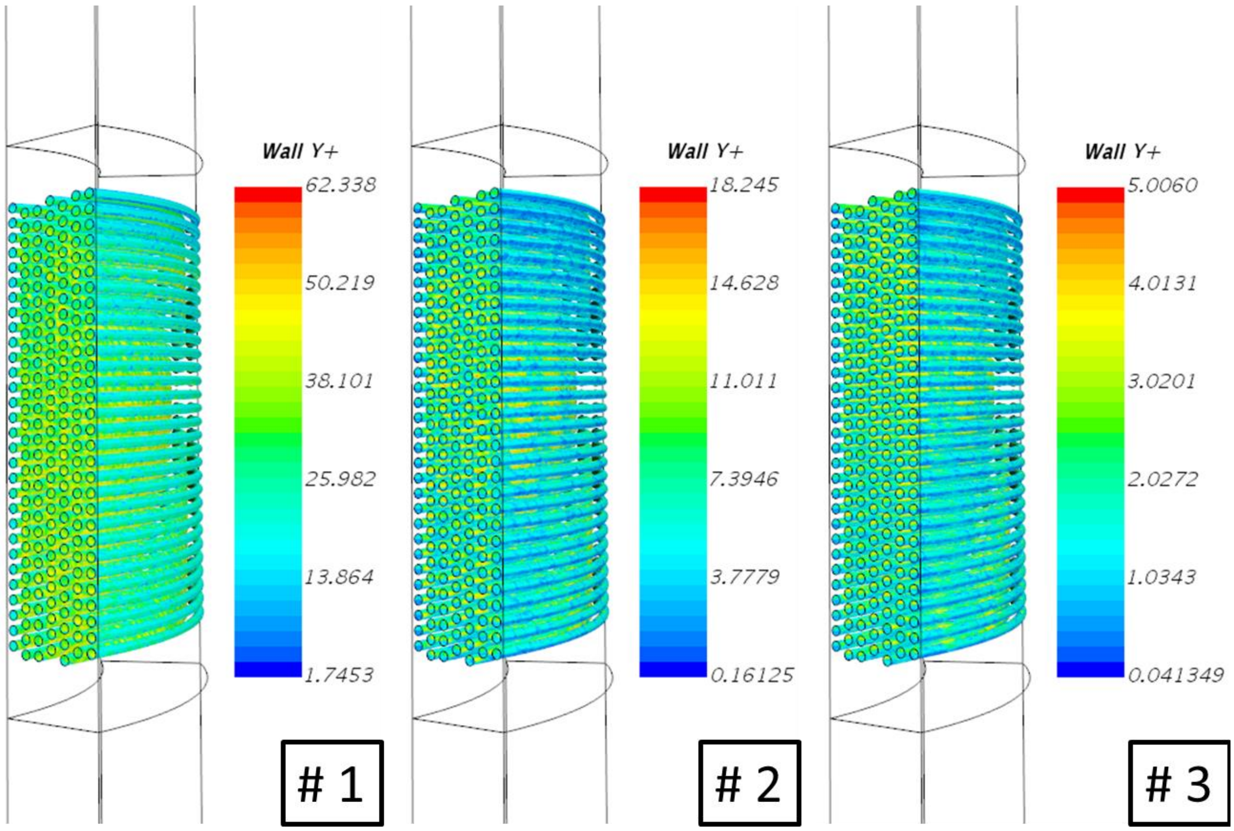

Figure 5. Wall y^+ distributions for different mesh configurations. The ranges in the figures are based on the maximum and minimum values in the simulations.

4. Results and discussion

In this section, results from various URANS models are analyzed in the context of the reference LES solution. Some insights on the applicability of the turbulence model and the choice of wall treatment are gained through the comparison and the candidate turbulence model is proposed for future application on the steam generator analysis.

4.1. Pressure drop

The pressure drops across the helical tube bundle for different turbulence models are provided in Table II. The URANS models coupled to a coarse boundary layer ($y^+ > 30$) visibly underestimate the predicted pressure drops. The realizable $k - \varepsilon$, linear standard $k - \varepsilon$, and the lag EB model have the top 3 predictions (within ~9%, 10%, and 17% respectively). Of these, the realizable and standard $k-\varepsilon$ models rely upon the linear isotropic assumption, while the lag EB model is built upon a non-isotropic turbulence assumption. Surprisingly, turbulence models resolving additional turbulence (SST and STRUCT) or based on more realistic formulations, such as the anisotropic turbulence assumptions (cubic $k-\varepsilon$ and STRUCT), show worse predictions of the pressure drop, which indicates that something is amiss in the simulations. However, when the near wall flow separation is resolved adopting the 2-layer representation, both STRUCT and the standard $k-\varepsilon$ cubic model predict the reference LES calculated pressure drop within 0.5%, and the cubic $k-\varepsilon$ model shows the best agreement with the LES solution. The linear standard $k-\varepsilon$ model can only gain marginal improvement from the improved wall resolution, as its isotropic stress assumption still produces overprediction of the turbulent viscosity and incorrect separation.

It is evident that for this flow configuration it is necessary to resolve the correct separation location: using wall functions and coarse wall boundary layers produces an incorrect separation location, which causes an unphysical flow bypass in the open region and the severe under prediction of pressure drops. Information about computational cost with different turbulence models is also provided. With the same coarsest boundary layer, STRUCT increases computational cost by 25% compared to the standard $k-\varepsilon$ linear model which has the lowest computational cost among all the mesh configurations and the selection of turbulence models. The STRUCT model with finest boundary layer shows a 51% larger cost than the standard $k-\varepsilon$ linear model with the coarsest boundary layer. Direct comparison between LES and RANS-based turbulence models was not possible due to the very different performance of individual CPUs and communication hardware adopted.

Table 2.

Computed pressure drop across the helical tube bundle for different turbulence models.

Turbulence models	Mesh configuration (given in Table 1)	Computational cost (CPU-hours)	Pressure drop (kPa)	Relative difference from LES (%)
LES (ANL)	-	N/A	6	0
Standard $k-\varepsilon$ cubic	#3	4211	6.01	0.1
STRUCT	#3	4864	5.97	0.5
STRUCT	#2	4333	6.12	2.0
Standard $k-\varepsilon$ linear	#3	3678	5.59	6.8
Realizable $k-\varepsilon$	#1	2935	5.44	9.3
Standard $k-\varepsilon$ linear	#1	2871	5.37	10.5
Lag EB	#1	3692	5.00	16.7
Standard $k-\varepsilon$ cubic	#1	3366	4.13	31.2
SST	#1	3191	3.82	36.3
STRUCT	#1	3709	3.43	42.8

4.2. Flow variance

The total turbulent kinetic energy defined in Eq. (4), containing both the resolved and the modeled portions, is shown in Figure 6 for channels 1, 2, 4, and 6. The inflow makes his way through the steam generator from top to bottom in the axial direction, corresponding to right to left in the figures. As expected, the URANS models underestimate the turbulent kinetic energy due to flow fluctuations when compared to the reference LES data. While the URANS models reasonably predict the steep increase in the velocity fluctuations at the top of the bundle, the turbulence in the bundle region decays to an equilibrium level below that seen in the LES results. Among the various models, the STRUCT model with fine boundary layer (y^+~1, mesh #3) generates the best predictions of turbulent kinetic energy. The solutions from the STRUCT model with intermediate boundary layer (y^+~6, mesh #2), standard linear $k-\varepsilon$, realizable $k-\varepsilon$ and lag EB models generally over predict modeled TKE, while under predicting total TKE. The SST, standard $k-\varepsilon$ cubic and STRUCT with coarse boundary layer (y^+~32, mesh #1) have the worst agreement. The standard $k-\varepsilon$ cubic naturally predicts lower TKE to reflect the true flow behavior, while it does not resolve all the unsteadiness for this case. Separate tests of standard $k-\varepsilon$ cubic and standard

$k - \varepsilon$ linear on the finest boundary layer (y^+~1, mesh #3) exhibit worse results for these models in comparison to the coarse boundary layer cases. This behavior is explained by the fact that while the RANS nature of the models leads them to significantly underpredict the levels of turbulence, the adoption of wall functions introduces artificial overprediction of the TKE levels near the wall, bringing the overall TKE values closer to the magnitude of the reference LES solutions.

The analysis of the results underlines the modeling challenge introduced by the aligned tube configuration (see Figure 7(a)), where the flow separation at the tube wall has dominant influence on the overall level of flow unsteadiness. Appropriate resolution of the boundary layer (y^+~1, mesh #3) is required to correctly predict the separation point, and the ability to resolve the transient turbulent structures detaching from the separation point is required to capture the dominant contribution of the resolved turbulence.

Based on the results obtained, the STRUCT model with fully resolved wall boundary layer (y^+~1, mesh #3) is the recommended approach for simulating the flow behavior, including turbulence levels, for this particular geometry while additional studies can be performed for the radially staggered geometry.

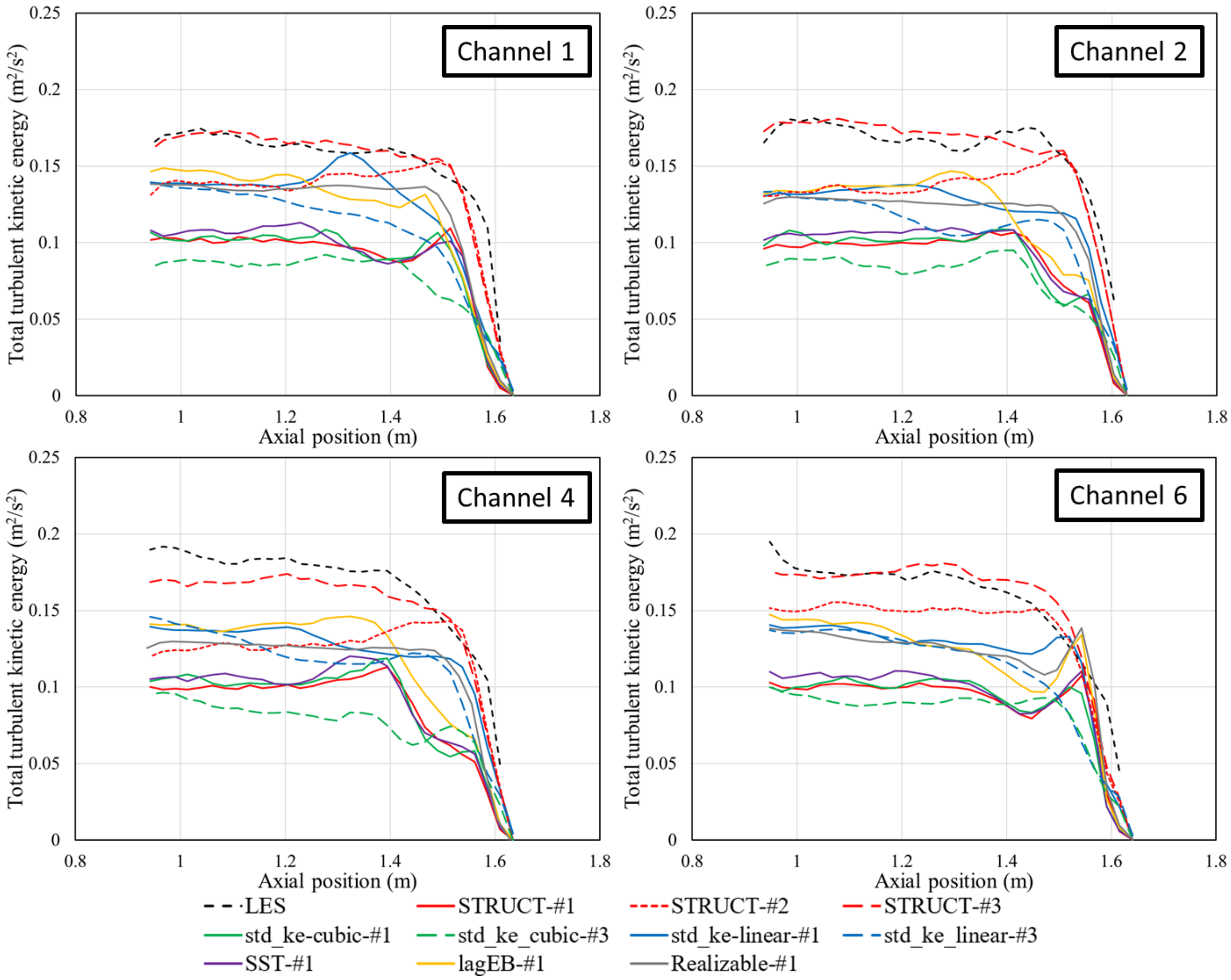

Figure 6. Comparison of total (resolved+modeled) turbulent kinetic energy for different turbulence models, where STRUCT-#1, #2, and #3 represent the three mesh configurations defined in Table 1 and std_ke stands for standard $k - \varepsilon$.

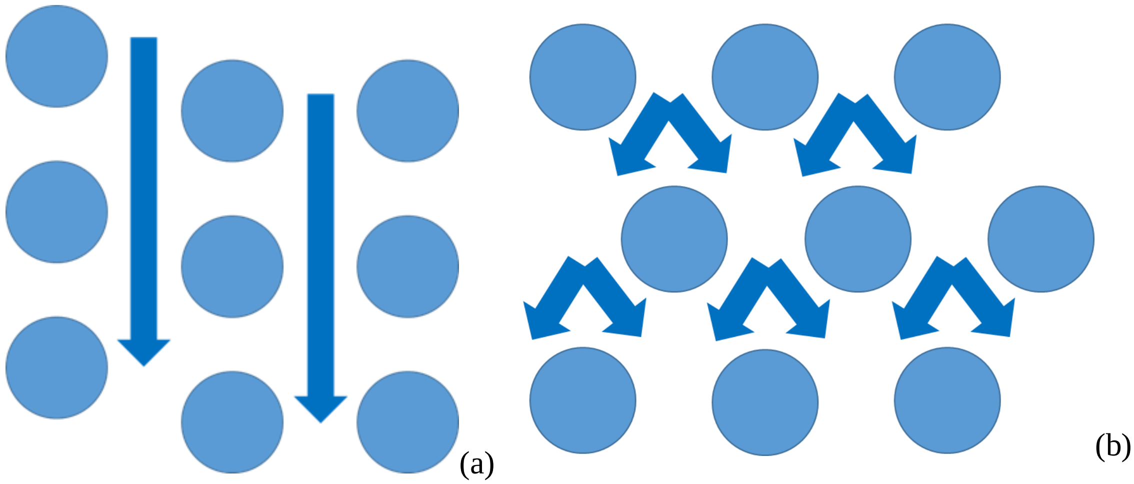

Figure 7. Illustration of the tested helical tube arrangement (a) and the axially-staggered helical tube arrangement (b).

4.3. Velocity field

Figure 8 shows the mean and instantaneous velocity magnitudes across the helical tube bundle. In **Figure 8,** for all the turbulence models with coarse boundary layers (y^+~32, mesh #1), the region of maximum velocity magnitude occurs on the left and right shoulders (approximately 90^{o} with respect to the flow direction). The transition of the velocity field from tube surface to the bulk is noticeably steep. As the near wall flow behavior is resolved, the velocity fields for the STRUCT with intermediate (y^+~6, mesh #2) and fine (y^+~1, mesh #3) wall boundary resolutions show relatively smoother transition. Similar trends are also observed for the standard $k - \varepsilon$ cubic model with fine (mesh #3) boundary layer.

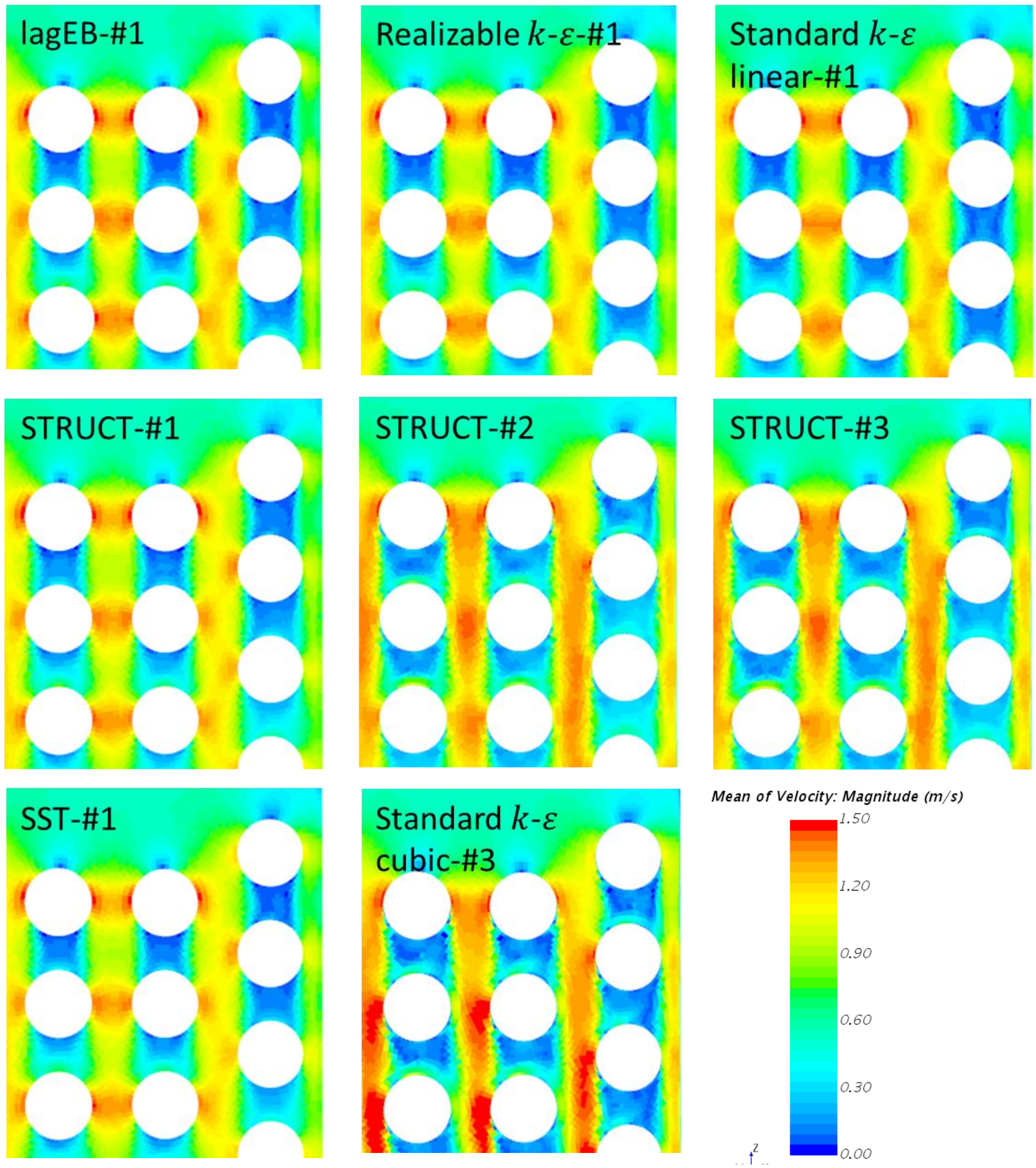

Figure 8. Cross-sectional views of the mean velocity magnitude across the small portions of helical tube bundle. Row 1 (left to right): lag EB-#1, realizable $k-\varepsilon$-#1, and standard $k-\varepsilon$ linear-#1. Row 2 (left to right): STRUCT-#1, STRUCT-#2 and STRUCT-#3. Row 3 (left to right): SST-#1 and standard $k-\varepsilon$ cubic-#3.

Figure 9 shows the integral line convolution of the instantaneous velocity vectors across the helical tube bundle, which allows to better appreciate the discussed flow separation effects. From **Figure 9** it is observed that for the first row of tubes all turbulence models are able to capture backflow behind the separation points, which is however not the case as the flow moves down in helical coil. **Figure 10** compares the distributions of the instantaneous velocity vectors on a larger portion of the helical tube bundle for the standard $k-\varepsilon$ cubic-#1, standard $k-\varepsilon$ cubic-#3 and the STRUCT-#3. It is observed that all models applied in combination to a wall function fail to capture the backflow and unsteadiness in the downstream region. As the near wall flow behavior is resolved with sufficient fine mesh (#3), both the standard $k-\varepsilon$ cubic and STRUCT models can better resolve the large recirculation areas, therefore providing considerably improved prediction accuracy in comparison to the wall function approach.

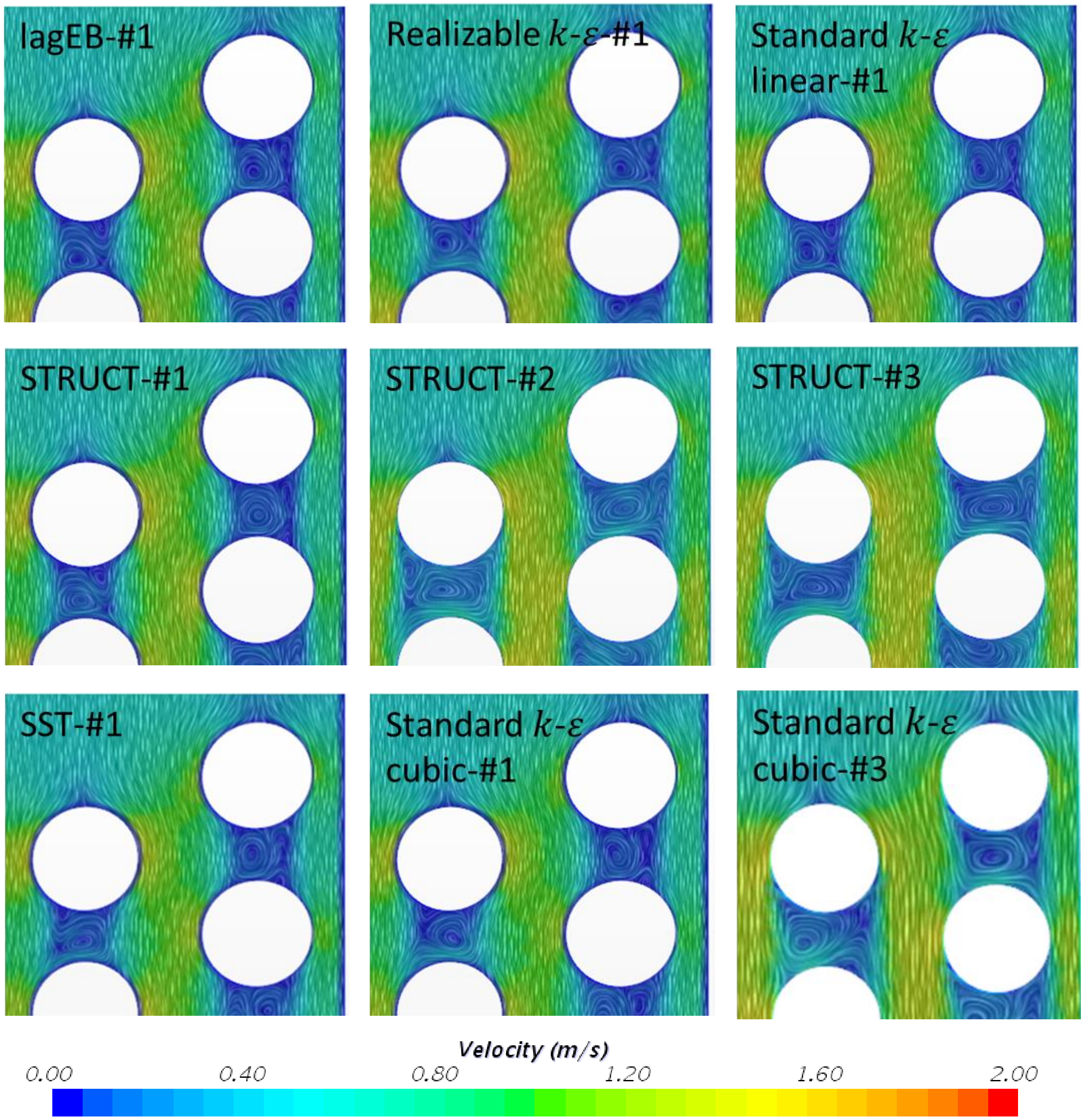

Figure 9. Cross-sectional view of the instantaneous velocity magnitude across a small portions of helical tube bundle. Row 1 (left to right): lag EB, realizable $k-\varepsilon$, and standard $k-\varepsilon$ linear. Row 2 (left to right): STRUCT-#1, STRUCT-#2 and STRUCT-#3. Row 3 (left to right): SST and standard $k-\varepsilon$ cubic.

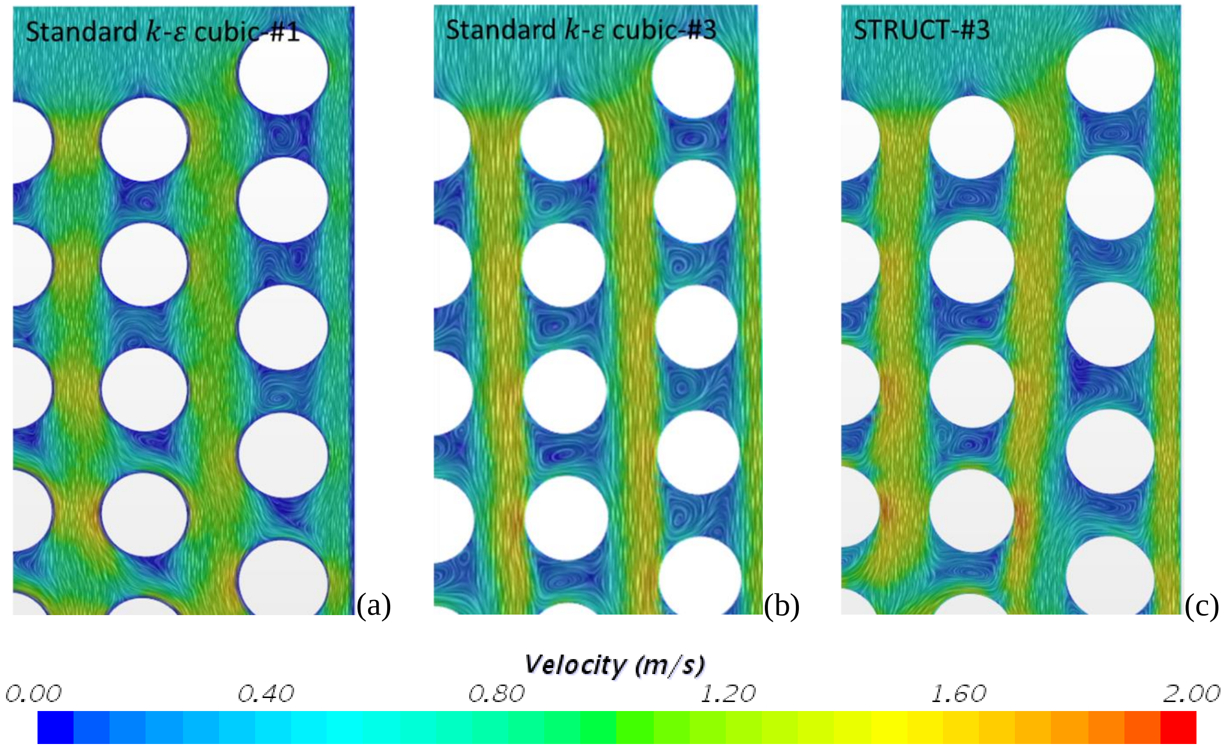

Figure 10. Cross-sectional view of the instantaneous velocity magnitude across the helical tube bundle. Left to Right: standard $k-\varepsilon$ cubic-#1 (a), standard $k-\varepsilon$ cubic-#3 (b) and STRUCT-#3 (b).

Figure 11 shows the instantaneous velocity fields at a representative downstream horizontal plane. As the flow passes through the helical tube bundle, RANS models tend to predict a decay in the velocity fluctuations for the downstream locations. This artificial damping is particularly severe for classic isotropic formulations, such as the standard $k-\varepsilon$ linear and realizable $k-\varepsilon$ models, where large high velocity regions form, confirming their expected inability to capture flow unsteadiness. Models that account for anisotropic effect such as the lagEB and the standard $k-\varepsilon$ cubic and STRUCT, can better resolve the smaller flow structures in the downstream region. The SST model can also resolve some of the flow features taking advantage of the clever limiting of turbulent viscosity overprediction in complex strains.

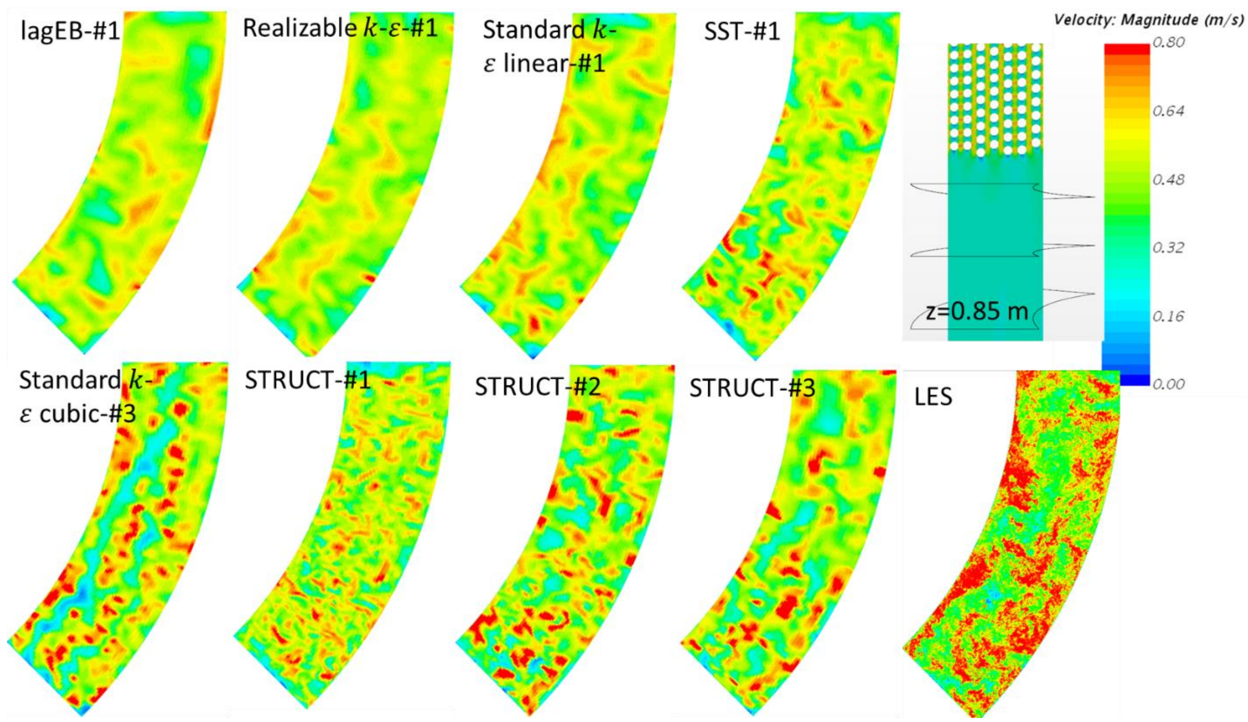

Figure 11. Distribution of the instantaneous velocity magnitude at z=0.85 m. Row 1 (left to right): lag EB-#1, realizable $k-\varepsilon$-#1, standard $k-\varepsilon$ linear-#1, and SST-#1. Row 2 (left to right): standard $k-\varepsilon$ cubic-#1, STRUCT-#1, STRUCT-#2, STRUCT-#3 and LES.

5. Conclusions

Accurate prediction of the flow behavior around helical steam generators coils requires special attention and bares considerable value to support the design of a number of advance nuclear plant concepts. In this paper, the most widely adopted URANS turbulence models and a recently proposed second-generation URANS model, STRUCT, have been assessed on the cross flow around a helical-coil tube bundles with rod based Reynolds number of 20,352. The solutions from the URANS models have been qualitatively and quantitatively compared to the reference LES reference solution data in respect to the global pressure drop and local volume-averaged turbulent kinetic energy predictions. Comparisons have also been presented for the velocity fields produced by the different models. For the investigated in line tube bundle arrangement the flow separation primarily occurs on the tube surface, and strongly affects the flow distribution in the whole system. Resolution of the near wall region is necessary in order to capture the separation, and a low cost near wall refinement combined with a two-layer near wall treatment provides satisfactory performance. Both the $k - \varepsilon$ cubic URANS model and the STRUCT model in combination with the two layer near wall treatment can provide excellent predictions of pressure drop in the analyzed configuration, with a relative difference within 0.5% in comparison to the LES solution.

Prediction of the turbulence levels is of outmost importance for flow induced vibration assessment in heat exchangers. In this regard URANS approaches are not able to resolve sufficient unsteadiness in the flow and underestimate the total turbulent kinetic energy in comparison to the LES solution. The solution of the STRUCT model coupled to the resolved boundary layer confirms the expected ability to resolve unsteady flow structures, predicting turbulence levels in good agreement with the LES results. The computational cost of the STRUCT approach remains comparable to the URANS methods, with a 25% increase on the same mesh finesse deriving from the cubic stress strain formulation and the additional transport equation.

It is noted that the combination of an inappropriate wall function approach with either the standard $k - \varepsilon$ linear or the realizable $k - \varepsilon$ models provides unexpectedly close predictions of the pressure drop and the total turbulent kinetic energy as a compensation phenomenon where the non-physical overproduction of modeled turbulent kinetic energy is counteracted by the inaccurate flow trajectories and the limited interaction with the helical coils in this specific configuration.

Acknowledgement

This work was funded under the auspices of the Nuclear Energy Advanced Modeling and Simulation (NEAMS) program of the U.S. Department of Energy, Office of Nuclear Energy. We also appreciate the support from the Argonne Leadership Computing Facility (ALCF) at Argonne National Laboratory which makes the reference LES simulation possible.

Reference

STAR-CCM+, version 12.02. , 2017.

Baglietto, E., Ninokata, H., 2005. A turbulence model study for simulating flow inside tight lattice rod bundles. Nucl. Eng. Des. 235, 773-784.

Baglietto, E., Ninokata, H., 2006. Anisotropic eddy viscosity modeling for application to industrial engineering internal flows. International Journal of Transport Phenomena 8, 109.

Baglietto, E., Ninokata, H., Misawa, T., 2006. CFD and DNS methodologies development for fuel bundle simulations. Nucl. Eng. Des. 236, 1503-1510.

Boussinesq, J., 1877. Theorie de l'Ecoulement Tourbillant. Mem.Presentes par Divers Savants Acad.Sci.Inst.Fr 23, 46-50.

Carelli, M.D., Conway, L., Oriani, L., Petrović, B., Lombardi, C., Ricotti, M.E., Barroso, A., Collado, J., Cinotti, L., Todreas, N., 2004. The design and safety features of the IRIS reactor. Nucl. Eng. Des. 230, 151-167.

Chen, S., Jendrzejczyk, J., Wambsganss, M., 1983. Tube vibration in a half-scale sector model of a helical tube steam generator. J. Sound Vibrat. 91, 539-569.

Durbin, P., 1993. A Reynolds stress model for near-wall turbulence. J. Fluid Mech. 249, 465-498.

Feng, J., Baglietto, E., 2018a. Thermal mixing test for STRUCT benchmark, 1-121.

Feng, J., Frahi, T., Baglietto, E., 2018b. STRUCTure-based URANS simulations of thermal mixing in T-junctions. Nucl. Eng. Des. 340, 275-299.

Fisher, P.F., Lottes, J.W., Kerkemier, S.G., 2008. Nek5000 Web page .

Launder, B., Sharma, B., 1974. Application of the energy-dissipation model of turbulence to the calculation of flow near a spinning disc. Letters in heat and mass transfer 1, 131-137.

Lenci, G., 2016. A methodology based on local resolution of turbulent structures for effective modeling of unsteady flows, Ph.D. Thesis. Massachusetts Institute of Technology .

Lenci, G., Feng, J., Baglietto, E., 2019. A second-generation URANS closure scaled by turbulent structures (in preparation). International Journal of Heat and Mass Transfer .

Lien, F., Chen, W., Leschziner, M., 1996. Low-Reynolds-number eddy-viscosity modelling based on non-linear stress-strain/vorticity relations, in Anonymous Engineering Turbulence Modelling and Experiments, Volume 3. Elsevier, pp. 91-100.

Manceau, R., Hanjalić, K., 2002. Elliptic blending model: A new near-wall Reynolds-stress turbulence closure. Phys. Fluids 14, 744-754.

Menter, F.R., 1994. Two-equation eddy-viscosity turbulence models for engineering applications. AIAA J. 32, 1598-1605.

Merzari, E., Obabko, A., Fischer, P., Halford, N., Walker, J., Siegel, A., Yu, Y., 2017. Large-scale large eddy simulation of nuclear reactor flows: Issues and perspectives. Nucl. Eng. Des. 312, 86-98.

Pope, S., 1975. A more general effective-viscosity hypothesis. J. Fluid Mech. 72, 331-340.

Prabhanjan, D., Raghavan, G., Rennie, T., 2002. Comparison of heat transfer rates between a straight tube heat exchanger and a helically coiled heat exchanger. Int. Commun. Heat Mass Transfer 29, 185-191.

Revell, A., Benhamadouche, S., Craft, T., Laurence, D., 2006. A stress–strain lag eddy viscosity model for unsteady mean flow. Int J Heat Fluid Flow 27, 821-830.

Shih, T., Liou, W., Shabbir, A., Yang, Z., Zhu, J., 1994. A new k-epsilon eddy viscosity model for high Reynolds number turbulent flows: Model development and validation.

Shih, T., Zhu, J., Lumley, J.L., 1995. A new Reynolds stress algebraic equation model. Comput. Methods Appl. Mech. Eng. 125, 287-302.

Yuan, H., Solberg, J., Merzari, E., Kraus, A., Grindeanu, I., 2017. Flow-induced vibration analysis of a helical coil steam generator experiment using large eddy simulation. Nucl. Eng. Des. 322, 547-562.